

See discussions, stats, and author profiles for this publication at: <https://www.researchgate.net/publication/51214198>

Experimental and Theoretical Investigation of Topological and Energetic Characteristics of Sb Complexes Reversibly Binding Molecular Oxygen

ARTICLE in THE JOURNAL OF PHYSICAL CHEMISTRY A · JUNE 2011

Impact Factor: 2.69 · DOI: 10.1021/jp201833w · Source: PubMed

CITATIONS

12

READS

43

7 AUTHORS, INCLUDING:



[Christian Jelsch](#)

French National Centre for Scientific Research

129 PUBLICATIONS 1,997 CITATIONS

[SEE PROFILE](#)



[Benoit Guillot](#)

University of Lorraine

76 PUBLICATIONS 759 CITATIONS

[SEE PROFILE](#)



[Andrey I. Poddel'sky](#)

Russian Academy of Sciences

58 PUBLICATIONS 646 CITATIONS

[SEE PROFILE](#)



[Vladimir Cherkasov](#)

Russian Academy of Sciences

307 PUBLICATIONS 2,305 CITATIONS

[SEE PROFILE](#)

Experimental and Theoretical Investigation of Topological and Energetic Characteristics of Sb Complexes Reversibly Binding Molecular Oxygen

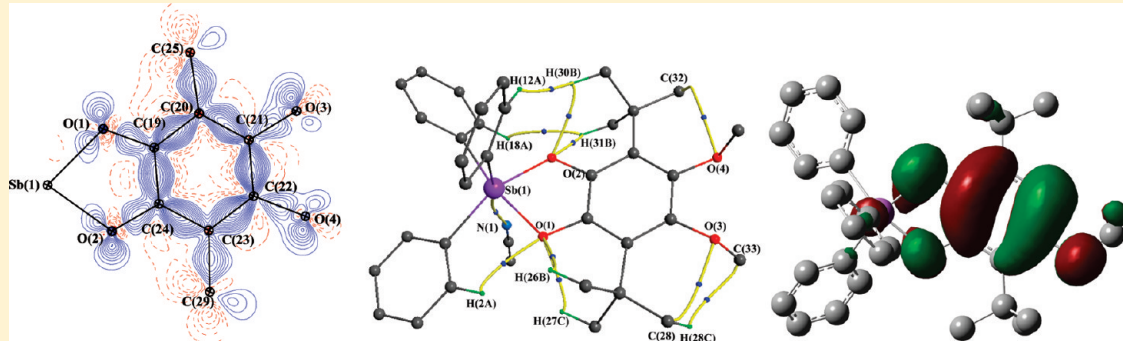
Georgy K. Fukin,^{*,†} Evgenii V. Baranov,[†] Christian Jelsch,[‡] Benoît Guillot,[‡] Andrey I. Poddel'sky,[†] Vladimir K. Cherkasov,[†] and Gleb A. Abakumov[†]

[†]G. A. Razuvayev Institute of Organometallic Chemistry of Russian Academy of Sciences, Tropinina 49, GSP-445, 603950 Nizhny Novgorod, Russia

[‡]Laboratoire de Crystallographie, Résonance Magnétique et Modélisations CRM2, CNRS, UMR 7036, Institut Jean Barriol, Faculté des Sciences et Technologies, Nancy University, BP 70239, 54506 Vandoeuvre-les-Nancy Cedex, France

Supporting Information

ABSTRACT:



The experimental distribution of electron density in $\text{Ph}_3(4,5\text{-OMe-3,6-Bu}^t\text{-Cat})\text{Sb}\cdot\text{MeCN}$ (**1***) and $\text{Ph}_3(4,5\text{-N}_2\text{C}_4\text{H}_6\text{-3,6-Bu}^t\text{-Cat})\text{Sb}\cdot\text{MeOH}$ (**2***) complexes was studied. According to atoms in molecules theory, the $\text{Sb}-\text{C}(\text{Ph})$, $\text{Sb}-\text{O}(\text{catecholate})$, and $\text{Sb}\cdots\text{N}(\text{O})$ bonds are intermediate, whereas the $\text{O}-\text{C}$ and $\text{C}-\text{C}$ bonds are covalent, respectively. The energy of the $\text{Sb}\cdots\text{N}(\text{MeCN})$ and $\text{Sb}\cdots\text{O}(\text{MeOH})$ bonds are 7.0 and 11.3 kcal/mol according to the Espinosa equation. Density functional theory and Hartree–Fock calculations were carried out for a series of catecholate and amidophenolate complexes of antimony(V). It was shown that such calculations reliably reproduce geometrical and topological parameters and therefore can be used for a criterion search of dioxygen reversible binding by the catecholate and amidophenolate complexes of antimony(V). It was found that the “critical” value of the HOMO energy vary in the range from -5.197 to -5.061 eV for reversible binding of dioxygen complexes. This can serve as a thermodynamic criterion to predict the possibility of the dioxygen reversible binding by the catecholate and amidophenolate complexes of Sb(V). The HOMO energies correlate with the conversion of the catecholate and amidophenolate complexes in corresponding spiroendoperoxide derivatives as well. The contribution of the atom orbitals of the carbon atoms in the five-membered metallocycle to HOMO in complexes with different substituents in the 4- and 5-positions of the catecholate ligand allows predicting the place of dioxygen addition.

INTRODUCTION

Recently, we have found the first examples of reversible dioxygen binding by non-transition-metal complexes: catecholatotriphenylantimony(V) (Ph_3SbCat) and *o*-amidophenolatotriphenylantimony(V) (Ph_3SbAP).^{1–4} The oxidation number of antimony(V) in catecholate and amidophenolate complexes remains unchanged upon dioxygen binding, in contrast to transition-metal complexes where similar phenomena take place.^{5,6} This is caused by one-electron oxidation of Cat (AP) ligands but not metal atoms, as it occurs with transition metal complexes (Scheme 1).

Therefore, it is of interest to study topological and energetic characteristics of Ph_3SbCat and Ph_3SbAP complexes in order to define clearly the main parameters of the complexes driving this process.

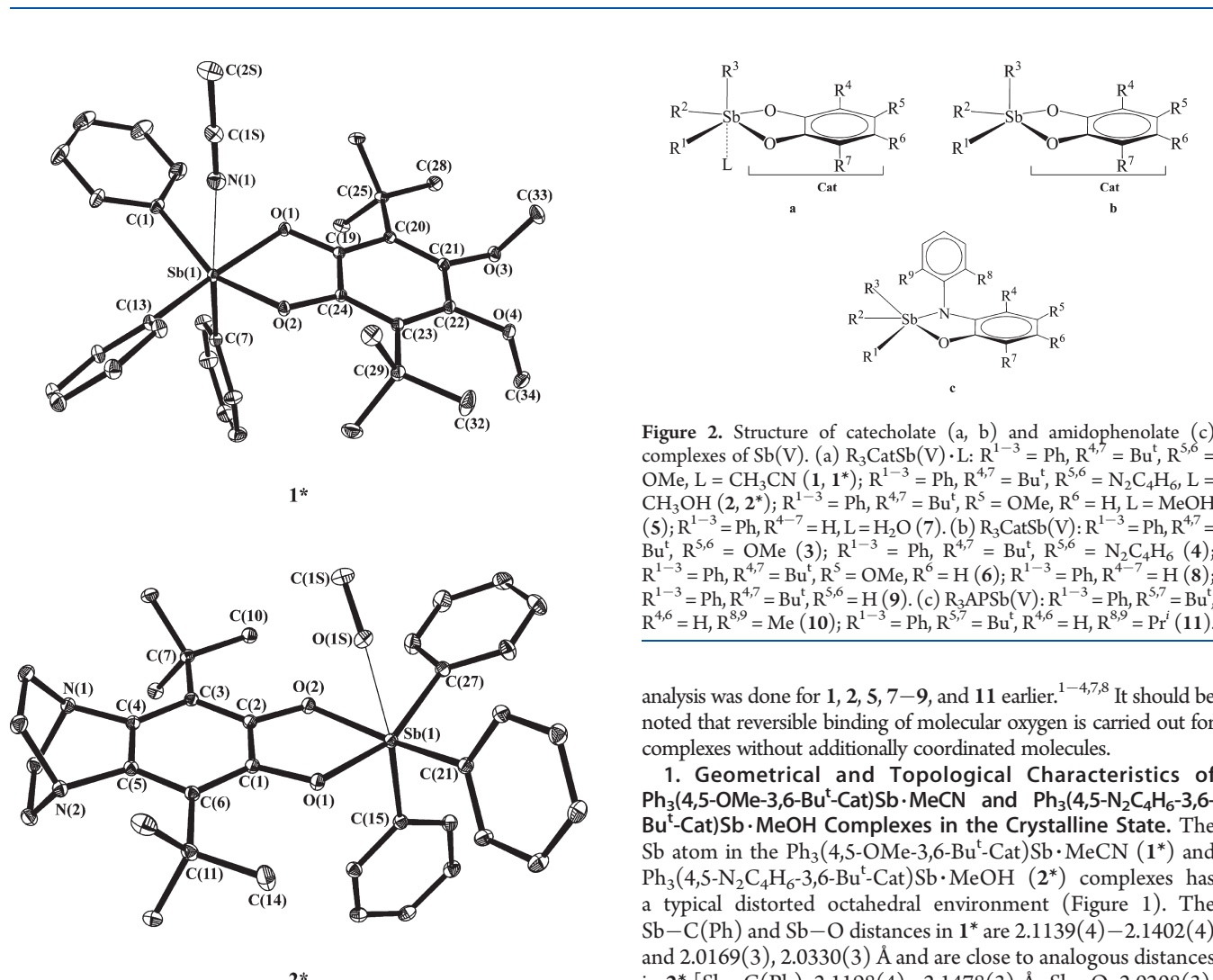
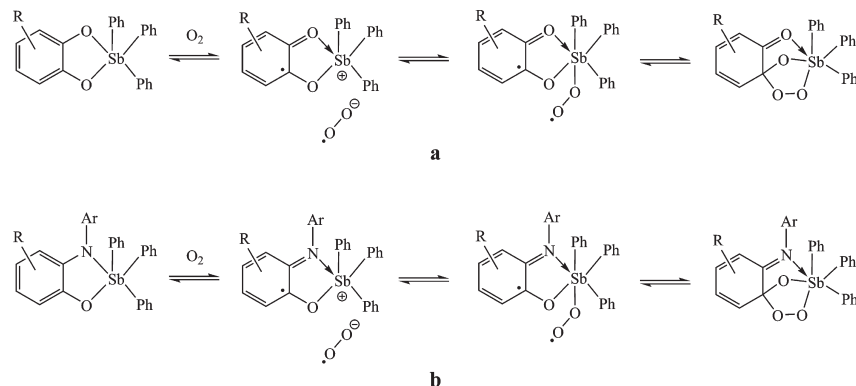
DISCUSSION

We carried out high-resolution X-ray diffraction experiments of the $\text{Ph}_3(4,5\text{-OMe-3,6-Bu}^t\text{-Cat})\text{Sb}\cdot\text{MeCN}$ (**1***) and $\text{Ph}_3(4,5\text{-N}_2\text{C}_4\text{H}_6\text{-3,6-Bu}^t\text{-Cat})\text{Sb}\cdot\text{MeOH}$ (**2***) complexes (Figure 1). In addition, quantum chemical calculations of the $\text{Ph}_3(4,5\text{-OMe-3,6-Bu}^t\text{-Cat})\text{Sb}\cdot\text{MeCN}$ (**1**), $\text{Ph}_3(4,5\text{-N}_2\text{C}_4\text{H}_6\text{-3,6-Bu}^t\text{-Cat})\text{Sb}\cdot\text{MeOH}$ (**2**), $\text{Ph}_3(4,5\text{-OMe-3,6-Bu}^t\text{-Cat})\text{Sb}$ (**3**), $\text{Ph}_3(4,5\text{-N}_2\text{C}_4\text{H}_6\text{-3,6-Bu}^t\text{-Cat})\text{Sb}$ (**4**), $\text{Ph}_3(4\text{-OMe-3,6-Bu}^t\text{-Cat})\text{Sb}\cdot\text{MeOH}$ (**5**), $\text{Ph}_3(4\text{-OMe-3,6-Bu}^t\text{-Cat})\text{Sb}$ (**6**), $\text{Ph}_3\text{CatSb}\cdot\text{H}_2\text{O}$ (**7**),

Received: February 24, 2011

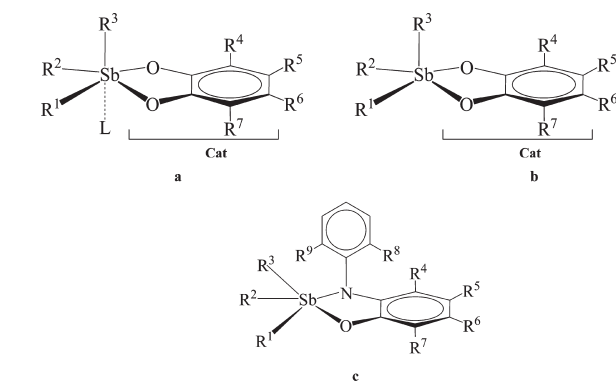
Revised: June 7, 2011

Published: June 13, 2011

Scheme 1. Reversible Binding of Dioxygen in Ph_3SbCat (a) and Ph_3SbAP (b) Complexes²**Figure 1.** Molecular structure of the $\text{Ph}_3(4,5\text{-OMe-3,6-Bu}^t\text{-Cat})\text{Sb}\cdot\text{MeCN}$ (**1***) and $\text{Ph}_3(4,5\text{-N}_2\text{C}_4\text{H}_6\text{-3,6-Bu}^t\text{-Cat})\text{Sb}\cdot\text{MeOH}$ (**2***) complexes.

Ph_3CatSb (**8**), $\text{Ph}_3(3,6\text{-Bu}^t\text{-Cat})\text{Sb}$ (**9**), $\text{Ph}_3(4,6\text{-Bu}^t\text{-AP}(2,6\text{-Me-Ph}))\text{Sb}$ (**10**), and $\text{Ph}_3(4,6\text{-Bu}^t\text{-AP}(2,6\text{-Pr}^i\text{-Ph}))\text{Sb}$ (**11**) compounds were performed (Figure 2).

Compounds **1–6**, **10**, and **11** bind reversibly the oxygen molecule, whereas compounds **7–9** are inert to O_2 . Routine X-ray

**Figure 2.** Structure of catecholate (a, b) and amidophenolate (c) complexes of $\text{Sb}(\text{V})$. (a) $\text{R}_3\text{CatSb}(\text{V})\cdot\text{L}$: $\text{R}^{1-3} = \text{Ph}$, $\text{R}^{4,7} = \text{Bu}^t$, $\text{R}^{5,6} = \text{OMe}$, $\text{L} = \text{CH}_3\text{CN}$ (**1**, **1***); $\text{R}^{1-3} = \text{Ph}$, $\text{R}^{4,7} = \text{Bu}^t$, $\text{R}^{5,6} = \text{N}_2\text{C}_4\text{H}_6$, $\text{L} = \text{CH}_3\text{OH}$ (**2**, **2***); $\text{R}^{1-3} = \text{Ph}$, $\text{R}^{4,7} = \text{Bu}^t$, $\text{R}^5 = \text{OMe}$, $\text{R}^6 = \text{H}$, $\text{L} = \text{MeOH}$ (**5**); $\text{R}^{1-3} = \text{Ph}$, $\text{R}^{4,7} = \text{H}$, $\text{L} = \text{H}_2\text{O}$ (**7**). (b) $\text{R}_3\text{CatSb}(\text{V})$: $\text{R}^{1-3} = \text{Ph}$, $\text{R}^{4,7} = \text{Bu}^t$, $\text{R}^{5,6} = \text{OMe}$ (**3**); $\text{R}^{1-3} = \text{Ph}$, $\text{R}^{4,7} = \text{Bu}^t$, $\text{R}^{5,6} = \text{N}_2\text{C}_4\text{H}_6$ (**4**); $\text{R}^{1-3} = \text{Ph}$, $\text{R}^{4,7} = \text{Bu}^t$, $\text{R}^5 = \text{OMe}$, $\text{R}^6 = \text{H}$ (**6**); $\text{R}^{1-3} = \text{Ph}$, $\text{R}^{4,7} = \text{H}$ (**8**); $\text{R}^{1-3} = \text{Ph}$, $\text{R}^{4,7} = \text{Bu}^t$, $\text{R}^{5,6} = \text{H}$ (**9**). (c) $\text{R}_3\text{APSb}(\text{V})$: $\text{R}^{1-3} = \text{Ph}$, $\text{R}^{5,7} = \text{Bu}^t$, $\text{R}^{4,6} = \text{H}$, $\text{R}^{8,9} = \text{Me}$ (**10**); $\text{R}^{1-3} = \text{Ph}$, $\text{R}^{5,7} = \text{Bu}^t$, $\text{R}^{4,6} = \text{H}$, $\text{R}^{8,9} = \text{Pr}^i$ (**11**).

analysis was done for **1**, **2**, **5**, **7–9**, and **11** earlier.^{1–4,7,8} It should be noted that reversible binding of molecular oxygen is carried out for complexes without additionally coordinated molecules.

1. Geometrical and Topological Characteristics of $\text{Ph}_3(4,5\text{-OMe-3,6-Bu}^t\text{-Cat})\text{Sb}\cdot\text{MeCN}$ and $\text{Ph}_3(4,5\text{-N}_2\text{C}_4\text{H}_6\text{-3,6-Bu}^t\text{-Cat})\text{Sb}\cdot\text{MeOH}$ Complexes in the Crystalline State. The Sb atom in the $\text{Ph}_3(4,5\text{-OMe-3,6-Bu}^t\text{-Cat})\text{Sb}\cdot\text{MeCN}$ (**1***) and $\text{Ph}_3(4,5\text{-N}_2\text{C}_4\text{H}_6\text{-3,6-Bu}^t\text{-Cat})\text{Sb}\cdot\text{MeOH}$ (**2***) complexes has a typical distorted octahedral environment (Figure 1). The $\text{Sb}-\text{C}(\text{Ph})$ and $\text{Sb}-\text{O}$ distances in **1*** are $2.1139(4)$ – $2.1402(4)$ and $2.0169(3)$, $2.0330(3)$ Å and are close to analogous distances in **2*** [$\text{Sb}-\text{C}(\text{Ph})$, $2.1198(4)$ – $2.1478(3)$ Å; $\text{Sb}-\text{O}$, $2.0208(3)$, $2.0305(3)$ Å]. It should be noted that the $\text{Sb}\cdots\text{N}(\text{MeCN})$ distance in **1*** [$2.7679(6)$ Å] significantly exceeds the $\text{Sb}\cdots\text{O}(\text{MeOH})$ distance in **2*** [$2.5117(4)$ Å]. Apparently, this leads to a noticeable difference in values of the dihedral angles between planes OSbO and OCOC . The dihedral angles between planes $\text{O}(1)-\text{Sb}(1)-\text{O}(2)$ and $\text{O}(1)-\text{C}(19)-\text{C}(24)-\text{O}(2)$ in **1*** is 16.6° , whereas a similar parameter in **2*** is equal to 0.4° . In both complexes, the Bu^t groups have eclipsed conformation. However, two Me groups of each Bu^t substituent are directed

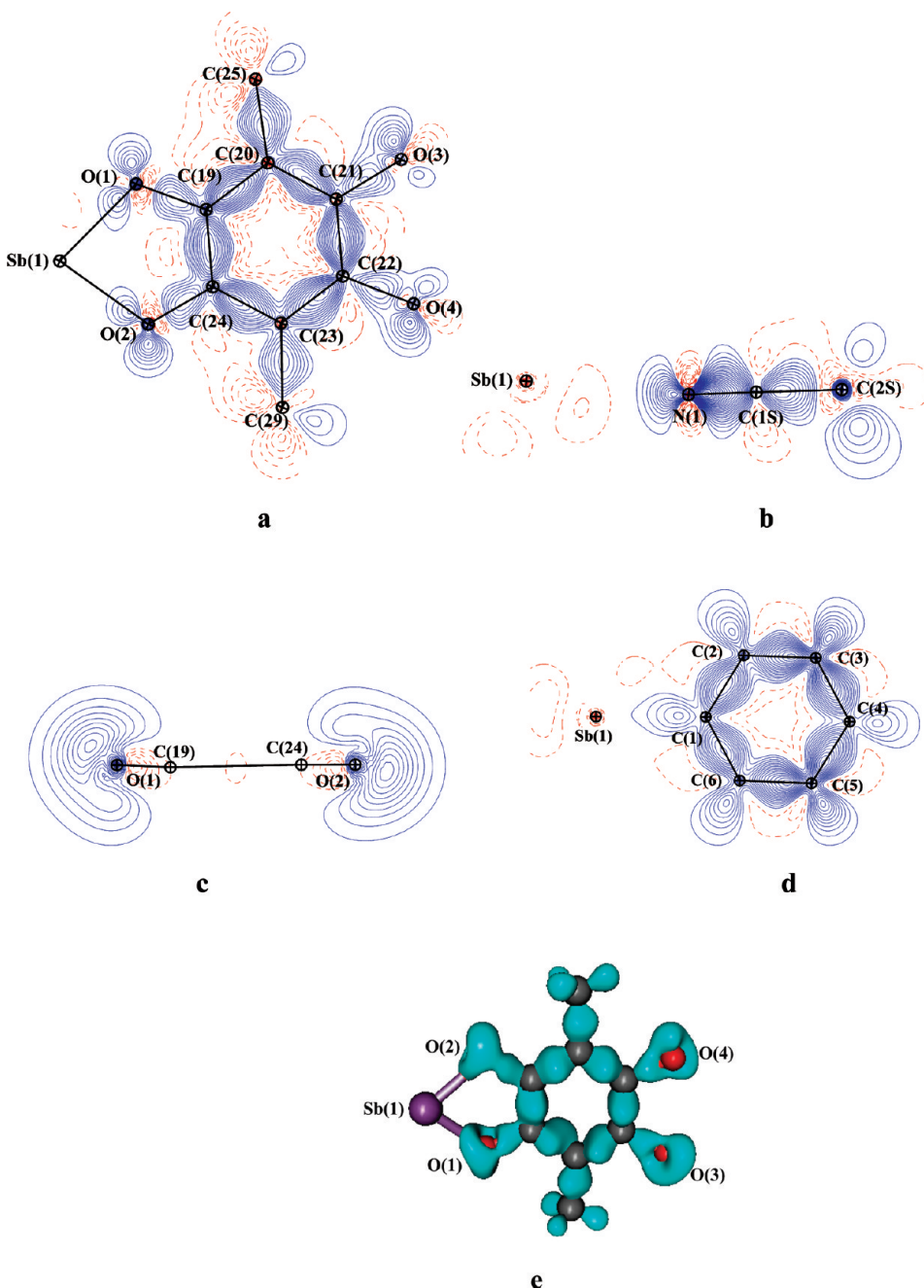


Figure 3. Experimental DED sections in $\mathbf{1}^*$ (contour $\pm 0.05 \text{ e}/\text{\AA}^3$): the plane of the benzene ring of the catecholate fragment (a); the plane of CH_3CN molecule (b); the plane containing the O(1) and O(2) atoms, which is perpendicular to the O(1)–C(19)–C(24)–O(2) fragment (c); the plane of the Ph ligand (d); and the envelope (0.01 au) of the catecholate ligand fragment (e). The solid lines (blue) show the concentration of DED, whereas the dashed lines (red) show the depletion of DED. H atoms are omitted for clarity.

to catecholate oxygen atoms in $\mathbf{1}^*$, whereas only one Me group is directed to catecholate oxygen atoms in $\mathbf{2}^*$. The O–C and C–C distances reflect the catecholate nature of corresponding ligands [O–C, 1.3538(5), 1.3552(5) Å in $\mathbf{1}^*$ and 1.3547(4), 1.3588(4) Å in $\mathbf{2}^*$; C–C, 1.4064(6)–1.4104(5) Å in $\mathbf{1}^*$ and 1.3985(4)–1.4277(4) Å in $\mathbf{2}^*$].

The distribution of deformation electron density (DED) for $\text{Sb}\cdots\text{ligand}$ bonds in $\mathbf{1}^*$ has explicitly pronounced polar (probably ionic) character (Figure 3). Maxima of DED for the O(1, 2)–C(19, 24) (Figure 3a), Sb–O(1, 2) (Figure 3a), Sb–N(CH_3CN) (Figure 3b), and Sb–C(Ph) (Figure 3d) bonds

are notably shifted to oxygen, carbon, and nitrogen atoms, respectively. Maxima of the DED on the Sb(1)–O(1, 2) and Sb–C(Ph) bonds are strictly directed toward the Sb(1) atom. The angles between the electron lone pairs of the catecholate oxygen atoms and the Sb–O and O–C bonds are close to 120° . The section in the plane containing the O(1) and O(2) atoms which is perpendicular to the O(1)–C(19)–C(24)–O(2) fragment shows only one maximum of electron density in each lone pair (Figure 3c). Apparently, the second maximum of electron density lone pair is shifted from the section plane. The similar distribution of DED is observed in $\mathbf{2}^*$ (Figure 4).

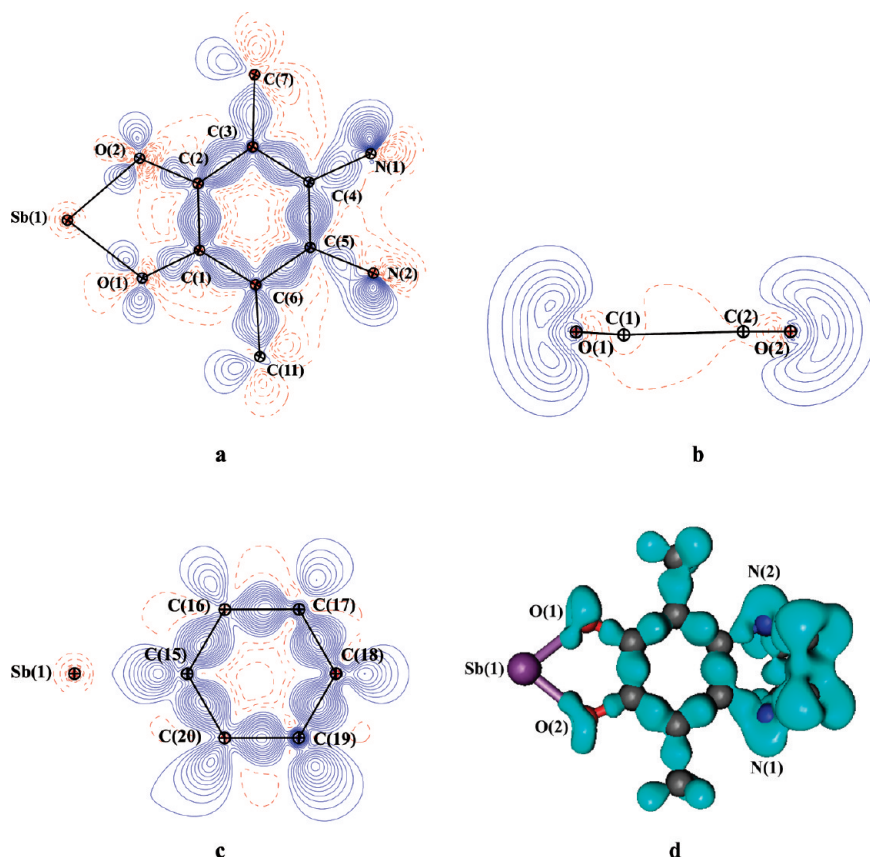


Figure 4. Experimental DED sections in 2^* (contour $\pm 0.05 \text{ e}/\text{\AA}^3$): the plane of the benzene ring of the catecholate fragment (a); the plane containing the O(1) and O(2) atoms, which is perpendicular to the O(1)-C(1)-C(2)-O(1) fragment (b); the plane of the Ph ligand (c); and the envelope (0.01 au) of the catecholate ligand fragment (d). The solid lines (blue) show the concentration of DED, whereas the dashed lines (red) show the depletion of DED. H atoms are omitted for clarity.

In contrast to 1^* , two maximum of lone pair at the O(1) atom are in the section plane (Figure 4b). The lone pairs of nitrogen atoms are positioned toward a “free” apex, and they form a tetrahedral environment around the N(1) and N(2) atoms (Figure 4a,d). It should be noted that the distribution of deformation electron density around six-coordinated antimony atoms in 1^* and 2^* shows an absence sp^3d^2 hybridization.

In order to understand the nature of chemical bonds in 1^* and 2^* (Table 1), we have used Bader theory.^{9,10} Corresponding calculations have shown that the Sb–O(catecholate), Sb–C(Ph), Sb \cdots N(CH₃CN), and Sb \cdots O(CH₃OH) bonds in 1^* and 2^* are intermediate interactions [$\nabla^2\rho(\mathbf{r}) > 0, h_e(\mathbf{r}) < 0$], whereas the O–C and C–C bonds within the catecholate fragments are shared interactions [covalent; $\nabla^2\rho(\mathbf{r}) < 0, h_e(\mathbf{r}) < 0$].

The presence of steric hindrance of Bu^t groups in ortho-positions to oxygen atoms allows us to suppose an existence of intramolecular O \cdots H interactions in molecules 1^* and 2^* . We calculated and built the molecular graph of 1^* and 2^* in order to visualize all intramolecular (interligand) interactions. We found that not only intramolecular interactions between the oxygen and hydrogen atoms of Bu^t groups exist (Table 2, Figure 5). Apart from the expected O \cdots H(Bu^t) interactions in 1^* , the C(Me) \cdots O, C(Me) \cdots H(Me), H(Ph) \cdots O, and H(Ph) \cdots H(Me) interactions were found. Unexpectedly, there are no O \cdots H(Bu^t) interactions in 2^* . Apparently, the O(1) \cdots H(2A, 26B, 27C) and O(2) \cdots H(30B, 31B) in 1^* and O(2) \cdots H(32), O(1S) \cdots H(26), N(1) \cdots H(12C, 13A),

and N(2) \cdots H(8A, 9B) in 2^* are caused by interactions between hydrogen and lone pairs of oxygen and nitrogen atoms. These interactions can be interpreted according to Popelier criteria as intramolecular hydrogen bonds.^{11,12} The hydrogen-acceptor distances in C–H \cdots O and C–H \cdots N interactions do not exceed the sum of van der Waals radii of corresponding atoms [$R(\text{O}) = 1.5 \text{ \AA}$, $R(\text{H}) = 1.2 \text{ \AA}$]¹³ (Table 2), and bond angles at the H atoms vary in the range of 113.3° – 123.7° and 120.8° – 123.2° , respectively. This statement agrees with the direction of the electron lone pairs of oxygen and nitrogen atoms (Figure 6). A similar situation takes place for the other C–H \cdots O and C–H \cdots N interactions in 1^* and 2^* . However, the intramolecular hydrogen bonds between the O(3), O(4) atoms in 1^* and the O(1), O(2) atoms in 2^* and the nearest hydrogen atoms are absent, in spite of appropriate O \cdots H distances (2.38 – 2.52 \AA). Analysis of the bond angles at these H atoms has shown that the C–H \cdots O angles vary in the range of 89.5° – 96.1° and that is significantly less than a typical range of angle values for hydrogen bonds (100° – 180°).¹⁴ Probably, this is by reason of an absence of the intramolecular hydrogen bonds between the O(3), O(4) atoms in 1^* and the O(1), O(2) atoms in 2^* and the nearest hydrogen atoms of the Bu^t groups.

It is interesting to note that the O(3)–C(21)–C(20)–C(25)–C(28), O(4)–C(22)–C(23)–C(29)–C(32) in 1^* and O(1)–C(1)–C(6)–C(11)–C(14), O(2)–C(2)–C(3)–C(7)–C(10) in 2^* fragments are planar (Figure 1). The deviation of these fragments from planarity are 0.011 \AA for O(3)–

Table 1. “Main Bond Distances and Topological Parameters in $\text{Ph}_3(4,5\text{-OMe-3,6-Bu}^t\text{-Cat})\text{Sb}\cdot\text{MeCN}$ (1^*) and $\text{Ph}_3(4,5\text{-N}_2\text{C}_4\text{H}_6\text{-3,6-Bu}^t\text{-Cat})\text{Sb}\cdot\text{MeOH}$ (2^*)

bond	distance, Å	$\nu(\mathbf{r}_{\text{cp}})$, au	$\rho(\mathbf{r}_{\text{cp}})$, au	$\nabla^2\rho(\mathbf{r}_{\text{cp}})$, au	$h_e(\mathbf{r}_{\text{cp}})$, au
1^*					
Sb(1)–O(1)	2.0330(3)	−0.166	0.107	0.334	−0.042
Sb(1)–O(2)	2.0169(3)	−0.164	0.105	0.353	−0.039
Sb(1)–N(1)	2.7679(6)	−0.022	0.031	0.058	−0.003
Sb(1)–C(1)	2.1288(4)	−0.121	0.091	0.196	−0.036
Sb(1)–C(7)	2.1139(4)	−0.153	0.108	0.136	−0.059
Sb(1)–C(13)	2.1402(4)	−0.144	0.106	0.110	−0.058
O(1)–C(19)	1.3538(5)	−0.763	0.311	−0.671	−0.468
O(2)–C(24)	1.3552(5)	−0.758	0.310	−0.670	−0.466
C(19)–C(24)	1.4104(5)	−0.728	0.304	−0.736	−0.456
C(19)–C(20)	1.4089(5)	−0.722	0.303	−0.757	−0.456
C(20)–C(21)	1.4064(6)	−0.447	0.300	−0.735	−0.447
C(21)–C(22)	1.4084(5)	−0.710	0.309	−0.736	−0.466
C(22)–C(23)	1.4082(5)	−0.719	0.301	−0.683	−0.445
C(23)–C(24)	1.4074(5)	−0.713	0.300	−0.676	−0.441
O(3)–C(21)	1.3839(5)	−0.697	0.295	−0.615	−0.425
O(4)–C(22)	1.3829(5)	−0.687	0.294	−0.682	−0.428
2^*					
Sb(1)–O(1)	2.0208(3)	−0.174	0.109	0.364	−0.041
Sb(1)–O(2)	2.0305(3)	−0.167	0.106	0.376	−0.036
Sb(1)–O(1S)	2.5117(4)	−0.036	0.041	0.103	−0.005
Sb(1)–C(15)	2.1198(4)	−0.179	0.119	0.172	−0.067
Sb(1)–C(21)	2.1478(3)	−0.155	0.110	0.123	−0.062
Sb(1)–C(27)	2.1439(3)	−0.153	0.108	0.145	−0.058
O(1)–C(1)	1.3588(4)	−0.737	0.307	−0.754	−0.462
O(2)–C(2)	1.3547(4)	−0.745	0.307	−0.662	−0.455
C(1)–C(2)	1.4277(4)	−0.698	0.297	−0.736	−0.441
C(2)–C(3)	1.4066(4)	−0.738	0.306	−0.721	−0.459
C(3)–C(4)	1.4140(4)	−0.692	0.294	−0.653	−0.427
C(4)–C(5)	1.3985(4)	−0.784	0.319	−0.873	−0.501
C(5)–C(6)	1.4134(4)	−0.704	0.298	−0.713	−0.441
C(1)–C(6)	1.4048(4)	−0.698	0.297	−0.732	−0.440
N(1)–C(4)	1.4527(4)	−0.613	0.270	−0.427	−0.359
N(1)–C(33)	1.4801(5)	−0.558	0.255	−0.356	−0.323
N(1)–C(35)	1.4814(5)	−0.510	0.243	−0.400	−0.305
N(2)–C(5)	1.4538(4)	−0.551	0.253	−0.377	−0.322
N(2)–C(34)	1.4809(5)	−0.607	0.268	−0.391	−0.352
N(2)–C(36)	1.4809(5)	−0.546	0.252	−0.370	−0.319

^aThe values of the local density of potential energy (ν), the total electron density (ρ), its Laplacian ($\nabla^2\rho$), and the local density of electronic energy (h_e) are shown at the bond critical points CP(3,−1).

C(21)–C(20)–C(25)–C(28), 0.017 Å for O(4)–C(22)–C(23)–C(29)–C(32), 0.015 Å for O(1)–C(1)–C(6)–C(11)–C(14), and 0.014 Å O(2)–C(2)–C(3)–C(7)–C(10) fragments. In other words, the interacting O···C atoms are located in the same plane and opposite to each other, whereas the corresponding H atoms are located out of plane. In order to understand the reason for C(Me)···O interactions in 1^* and 2^* , we built an appropriate section of DED and a Laplacian of the total electron density in 2^* (Figure 7). Around the C(14) atom is

Table 2. “Energy of Intramolecular Interactions in $\text{Ph}_3(4,5\text{-OMe-3,6-Bu}^t\text{-Cat})\text{Sb}\cdot\text{MeCN}$ (1^*) and $\text{Ph}_3(4,5\text{-N}_2\text{C}_4\text{H}_6\text{-3,6-Bu}^t\text{-Cat})\text{Sb}\cdot\text{MeOH}$ (2^*)

interaction	distance, Å	$\rho(\mathbf{r}_{\text{cp}})$, au	$\nabla^2\rho(\mathbf{r}_{\text{cp}})$, au	E , kcal/mol
1^*				
Sb(1)–N(1)	2.7679(6)	0.031	0.059	−7.0
O(1)–H(26B)	2.28	0.016	0.060	−3.3
O(1)–H(27C)	2.20	0.019	0.071	−4.3
O(1)–H(2A)	2.41	0.013	0.049	−2.5
O(2)–H(30B)	2.25	0.017	0.066	−3.8
O(2)–H(31B)	2.21	0.017	0.069	−3.9
H(30B)–H(12A)	2.33	0.005	0.019	−0.8
H(31B)–H(18A)	2.32	0.005	0.019	−0.7
O(4)–C(32)	2.7326(8)	0.020	0.073	−4.6
O(3)–C(28)	2.7208(7)	0.018	0.072	−4.1
C(33)–H(28C)	2.61	0.016	0.042	−3.0
2^*				
Sb(1)–O(1S)	2.5117(4)	0.041	0.104	−11.3
O(1)–C(14)	2.6787(5)	0.016	0.074	−3.8
O(2)–C(10)	2.7051(5)	0.017	0.071	−3.9
O(2)–H(32)	2.28	0.014	0.060	−3.0
C(10)–H(32)	2.61	0.009	0.037	−1.6
O(1S)–H(26)	2.45	0.013	0.041	−2.3
H(10A)–H(1SB)	2.31	0.005	0.022	−0.9
N(1)–H(9B)	2.32	0.019	0.064	−4.1
N(1)–H(8A)	2.41	0.014	0.053	−2.8
N(2)–H(12C)	2.38	0.015	0.058	−3.2
N(2)–H(13A)	2.39	0.014	0.055	−3.0

^aThe energy is derived from the Espinosa equation: $E = 1/2\nu(\mathbf{r}_{\text{cp}})$.

observed a typical depletion of DED, which is caused by the formation of the C–H bonds (Figure 7a–c). Zero isosurface of $\nabla^2\rho(\mathbf{r})$ shows an electron density local depletion (“hole”) near the C(14) nucleus as well (Figure 7d–f). Thus, realization of oxygen nucleophilic properties lead to the redistribution of ED between O(1) and C(14) atoms. Consequently, a weak electron accumulation appears between O(1) and C(14) atoms (Figure 5b), and a (3,−1) critical point is located in that region. Analogous situations take place for the other O···C(Me) and C(Me)···H(Me) and C(Me)···H(Ph) interactions in 1^* and 2^* .

The strongest interactions according to the Espinosa equation¹⁵ take place between the antimony atoms and additionally coordinated molecules of CH₃CN in 1^* (−7.0 kcal/mol) and CH₃OH in 2^* (−11.3 kcal/mol). The energy of intramolecular O···H and N···H interactions in 1^* and 2^* varies in the range from −2.5 to −4.3 kcal/mol and −2.8 to −4.1 kcal/mol, respectively, and such interactions can be interpreted as weak hydrogen bonds.¹⁴ According to topological parameters in CP(3,−1), all these interactions have an ionic nature [“closed shell” interactions, $\nabla^2\rho(\mathbf{r}) > 0$, $h_e(\mathbf{r}) > 0$].

2. Comparison of Geometrical and Topological Characteristics of Ph₃(4,5-OMe-3,6-Bu^t-Cat)Sb·MeCN Complex in Crystalline and Isolated States. Quantum chemical calculations are necessary in order to find a criterion that could be used for theoretical prediction of the dioxygen reversible binding to

the catecholate Sb(V) complexes. There are not many high-resolution X-ray experiments available for the catecholate Sb(V)

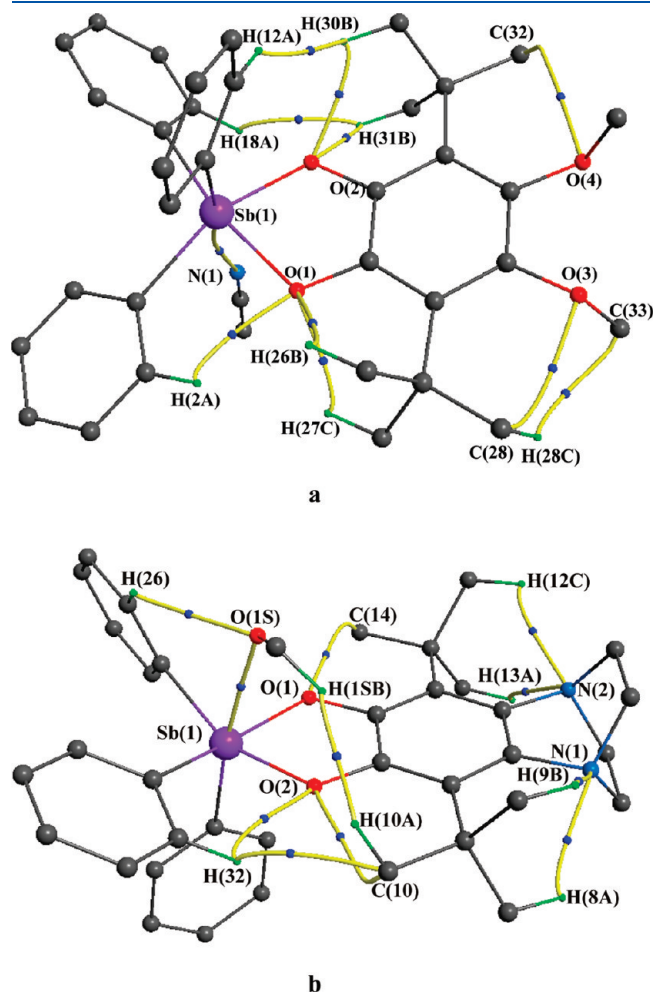


Figure 5. Only intramolecular bond paths and CP(3,-1) critical points are presented [(a) Ph₃(4,5-OMe-3,6-Bu^t-Cat)Sb·MeCN (1*), (b) Ph₃(4,5-N₂C₄H₆-3,6-Bu^t-Cat)Sb·MeOH (2*)]. The interacting atoms are labeled.

complexes. Also, the complexes 1* and 2* contain additionally coordinated CH₃CN and CH₃OH solvent molecules, whereas the dioxygen reversible binding was carried out for the catecholate Sb(V) complexes without coordinated molecules. Therefore, it is important to compare the geometrical and topological parameters for 1* obtained by the high-resolution X-ray experiment and DFT level with the hybrid B3LYP functional using the DGDZVP basis set and the program Gaussian 03.¹⁶

We focus our attention on the geometrical and topological characteristics of the five-membered SbOCCO metallocycle, because the process of reversible binding of dioxygen starts by oxidation of the catecholate (amidophenolate) ligand (Scheme 1). The numeration of catecholate fragment atoms in molecules is presented in Figure 8 (a, optimized by DFT and precise X-ray analysis of 2*; b, precise X-ray analysis of 1*), and the main geometrical and topological characteristics of the five-membered SbOCCO metallocycle calculated by DFT and AIM theory^{9,10} are presented in Table 3.

The distances within the SbOCCO fragment in 1* (Table 1) is slightly but systematically shorter than analogous distances in 1 (Table 3). Apparently, such a difference is caused by different aggregative states: molecules 1* are in crystalline state, whereas 1 corresponds to the gas phase. The Sb—C(Ph) distances in 1 and 1* reflect this tendency [2.1139(4)–2.1402(4) Å in 1* and 2.1524–2.1767 Å in 1] as well. The C—C distances in the catecholate ligands of 1* and 1 most closely correspond to each other [1.4064(6)–1.4104(5) Å in 1* and 1.4103–1.4153 Å in 1]. It should be noted that the Sb(1)—O(1, 2) distances both in crystal and in isolated state reveal some unequivalence. The largest differences in geometrical parameters in 1* and 1 are observed for bond lengths Sb···N(CH₃CN) and angles Sb—N—C. The Sb···N(CH₃CN) distances and Sb—N—C angles are 2.7679(6) Å, 173.34(5)° in 1* and 2.8947 Å, 146.15° in 1. Apparently, the coordinated CH₃CN molecule in crystal has a lower degree of freedom in comparison with the molecule in the isolated complex. Therefore, the Sb···N distances and Sb—N—C angles differ strongly in 1* and 1. Also, the electron density $\rho(\mathbf{r})$ at the CP(3,-1) in 1 (0.018 au) for the Sb(1)···N(1) bond is much lower than for the C—C bonds in the catecholate ligand (0.297–0.304 au). As a result, the catecholate ligand geometry

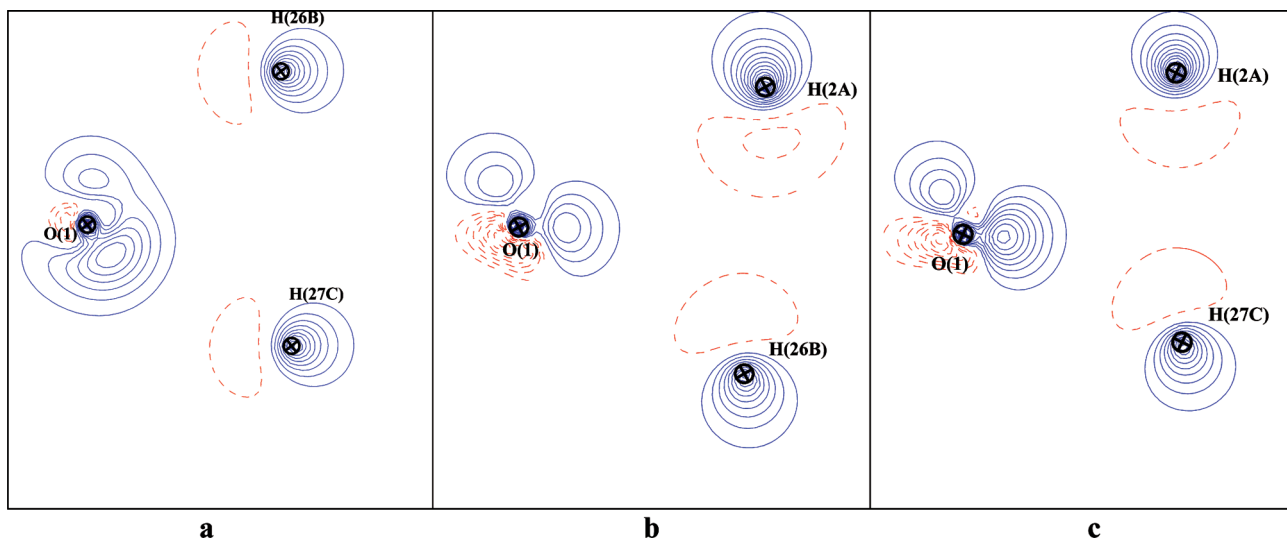


Figure 6. Experimental DED section in 1* (contour $\pm 0.05 \text{ e}/\text{\AA}^3$): the O(1)—H(26B)—H(27C) plane (a), the O(1)—H(2A)—H(26B) plane (b), the O(1)—H(2A)—H(27C) plane (c). The solid lines show the ED concentration, whereas the dashed lines show the ED depletion.

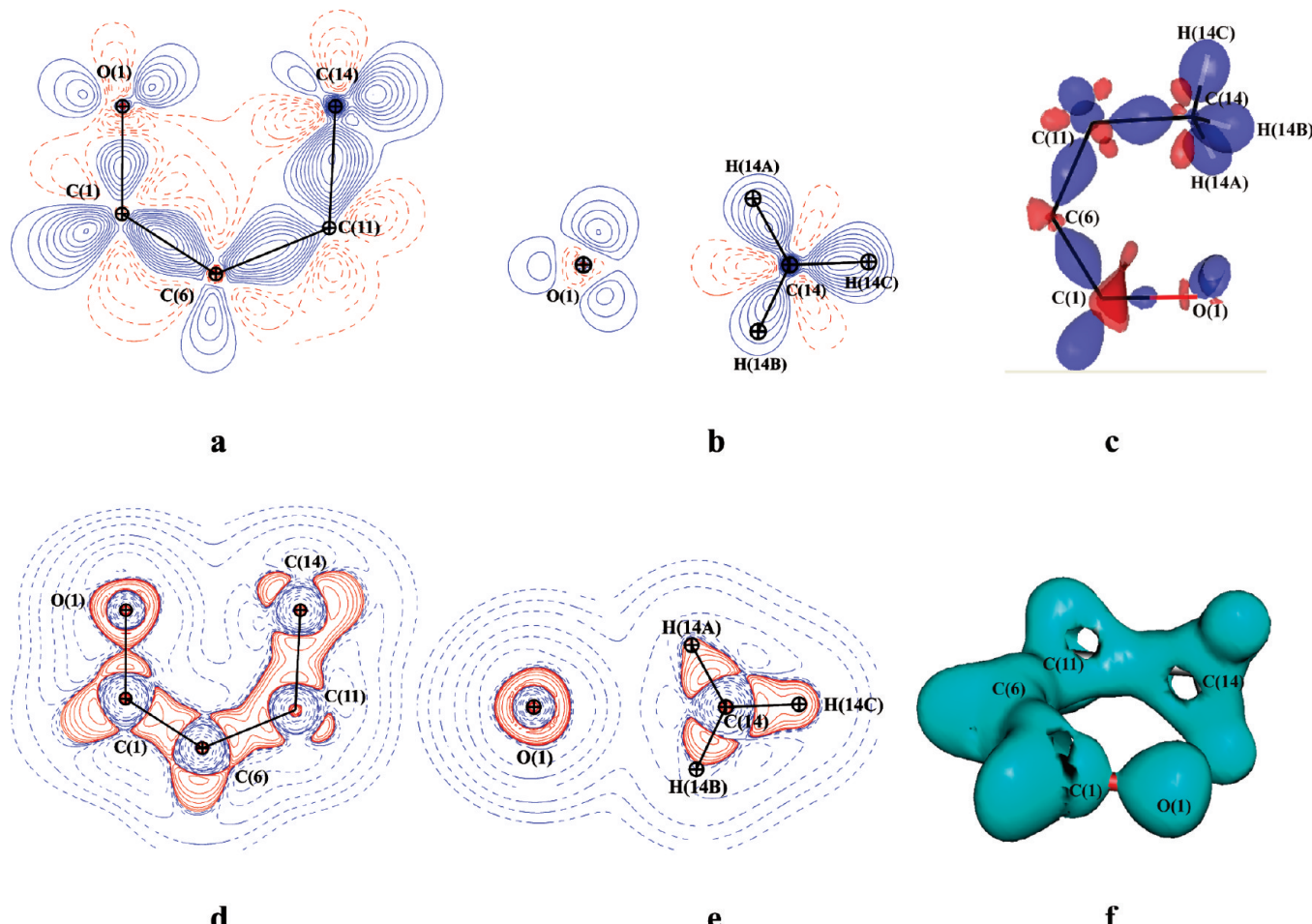


Figure 7. Experimental DED (contour $\pm 0.05 \text{ e}/\text{\AA}^3$) and Laplacian sections of the $\text{O}(1)-\text{C}(1)-\text{C}(6)-\text{C}(11)-\text{C}(14)$ fragment in 2^* : in the plane of the $\text{O}(1)-\text{C}(1)-\text{C}(6)-\text{C}(11)-\text{C}(14)$ fragment (a, DED; d, Laplacian of ED); the plane containing the $\text{O}(1)$ and $\text{C}(14)$ atoms, which is perpendicular to the $\text{O}(1)-\text{C}(1)-\text{C}(6)-\text{C}(11)-\text{C}(14)$ fragment (b, DED; e, Laplacian of ED); the envelope of the $\text{O}(1)-\text{C}(1)-\text{C}(6)-\text{C}(11)-\text{C}(14)$ fragment [c, DED (0.03 au); e, Laplacian of ED ($\nabla^2\rho(\mathbf{r}) = 0 \text{ au}$)]. The solid lines (blue) show the concentration of DED, whereas the dashed lines (red) show the depletion of DED. The solid lines (red) show the concentration of the ED Laplacian, whereas the dashed lines (blue) show the depletion of the ED Laplacian.

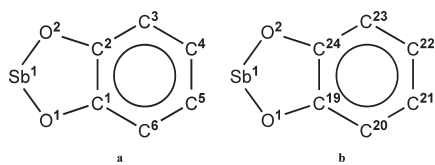


Figure 8. The numeration of the catecholate atoms for molecules (a) optimized by DFT calculations and the high-resolution X-ray experiment of 2^* and (b) the high-resolution X-ray experiment of 1^* .

is reproduced by DFT calculation more precisely than the $\text{Sb}(1)\cdots\text{N}(1)$ distance. Apparently, $\rho(\mathbf{r})$ in $\text{CP}(3,-1)$ can be a criterion of “hardness” or “softness” of a bond or ligand. A comparison of the 2^* and 2 geometric parameters shows the same tendency.

Thus, the quantum chemical optimization of the 1 geometry reproduces the geometry of the “rigid” fragments in 1^* better than that of the “soft” ones as well as in 2 and 2^* . Therefore, topological characteristics [$\rho(\mathbf{r}), \nabla^2\rho(\mathbf{r}), \nu(\mathbf{r}), h_e(\mathbf{r})$ in $\text{CP}(3,-1)$] of the SbOCCO fragment in crystalline and isolated states have similar values (Tables 1 and 3). According to AIM theory, the $\text{Sb}-\text{O}$, $\text{Sb}-\text{C}(\text{Ph})$ interactions are intermediate interactions,

whereas the $\text{O}-\text{C}$ and $\text{C}-\text{C}$ interactions are covalent, respectively (shared interactions). This statement agreed with information about the nature of the $\text{Sb}-\text{O}$, $\text{Sb}-\text{C}(\text{Ph})$, $\text{O}-\text{C}$, and $\text{C}-\text{C}$ bonds in the crystalline state of 1^* and 2^* . However, the $\text{Sb}\cdots\text{N}(\text{CH}_3\text{CN})$ and $\text{Sb}\cdots\text{O}(\text{MeOH})$ interactions in the crystal are intermediate, whereas these interactions according DFT calculation have a closed shell nature. Apparently, such a difference in the interaction types is caused by substantial difference in the $\text{Sb}\cdots\text{N}(\text{CH}_3\text{CN})$ and $\text{Sb}\cdots\text{O}(\text{MeOH})$ distances in crystalline and isolated states.

In contrast to 1 , the geometry of molecule 3 is optimized without an additional coordinated molecule of acetonitrile. Geometrical parameters of the SbOCCO fragment in 3 are close to those in 1 , at least they reflect unequivalence of the $\text{Sb}-\text{O}$ distances as well. The $\text{Sb}-\text{C}(\text{Ph})$, $\text{O}-\text{C}$, and $\text{C}-\text{C}$ distances in 3 are $2.1499-2.1801$, 1.3661 , 1.3799 , and $1.4097-1.4159 \text{ \AA}$, respectively. Interactions $\text{Sb}-\text{O}$ and $\text{Sb}-\text{C}(\text{Ph})$ in 3 are intermediate interactions, whereas the $\text{O}-\text{C}$ and $\text{C}-\text{C}$ bonds are covalent. The energy of the $\text{Sb}\cdots\text{N}(\text{CH}_3\text{CN})$ bond in 1 calculated as $E_{(\text{Ph}_3(4,5-\text{OMe}-3,6-\text{Bu}^t-\text{Cat})\text{Sb}\cdot\text{MeCN})} - (E_{(\text{Ph}_3(4,5-\text{OMe}-3,6-\text{Bu}^t-\text{Cat})\text{Sb}} + E_{(\text{MeCN})})$ is -4.6 kcal/mol , exceeding slightly the value calculated

from the correlation equation of Espinosa (-3.4 kcal/mol).¹⁵ Use of the Espinosa equation for a molecule in crystal (**1***) gives the $\text{Sb}\cdots\text{N}(\text{CH}_3\text{CN})$ bond energy (-7.0 kcal/mol) to be higher as compared to that in the isolated state. In the first order, the difference of the $\text{Sb}\cdots\text{N}$ energy in **1*** and **1** is caused by different $\text{Sb}\cdots\text{N}$ distances [$(2.7679(6)\text{ \AA}$ in **1*** and 2.8947 \AA in **1**) and respectively $\rho(\mathbf{r})$ in $\text{CP}(3,-1)$ (0.031 au in **1***, 0.018 au in **1**) and $\nu(\mathbf{r})$ in $\text{CP}(3,-1)$ (-0.022 au in **1***, -0.011 au in **1**). The same situation takes place for the **4** complex as compared to **2**. The energy of the $\text{Sb}\cdots\text{O}(\text{MeOH})$ bond in **2** calculated as

Table 3. Main Geometrical and Topological Characteristics for the Five-Membered SbOCCO Metallocycle in $\text{Ph}_3(4,5\text{-OMe-3,6-Bu}^t\text{-Cat})\text{Sb}\cdot\text{MeCN}$ (**1**) and $\text{Ph}_3(4,5\text{-OMe-3,6-Bu}^t\text{-Cat})\text{Sb}$ (**3**) According to DFT and AIM Theory^a

no.	bond	distance, \AA	$\rho(\mathbf{r}_{\text{cp}})$, au	$\nabla^2\rho(\mathbf{r}_{\text{cp}})$, au	$\nu(\mathbf{r}_{\text{cp}})$, au	$h_e(\mathbf{r}_{\text{cp}})$, au
1	Sb(1)–O(1)	2.0775	0.095	0.300	-0.139	-0.032
	Sb(1)–O(2)	2.0675	0.097	0.310	-0.144	-0.033
	O(1)–C(1)	1.3631	0.282	-0.357	-0.660	-0.374
	O(2)–C(2)	1.3674	0.280	-0.361	-0.649	-0.369
	C(1)–C(2)	1.4135	0.304	-0.915	-0.418	-0.323
3	Sb(1)–O(1)	2.0942	0.092	0.286	-0.133	-0.031
	Sb(1)–O(2)	2.0426	0.102	0.334	-0.156	-0.036
	O(1)–C(1)	1.3661	0.280	-0.360	-0.650	-0.370
	O(2)–C(2)	1.3799	0.270	-0.324	-0.621	-0.351
	C(1)–C(2)	1.4101	0.306	-0.925	-0.423	-0.327

^aThe values of the local density of potential energy (ν), the total electron density (ρ), its Laplacian ($\nabla^2\rho$), and the local density of electronic energy (h_e) are shown at the bond critical points $\text{CP}(3,-1)$.

$E_{(\text{Ph}_3(4,5\text{-N}_2\text{C}_4\text{H}_6\text{-3,6-Bu}^t\text{-Cat})\text{Sb}\cdot\text{MeOH})} - (E_{(\text{Ph}_3(4,5\text{-N}_2\text{C}_4\text{H}_6\text{-3,6-Bu}^t\text{-Cat})\text{Sb}} + E_{(\text{MeOH})})$ is -7.6 kcal/mol, whereas the correlation equation of Espinosa gives a value of -5.4 kcal/mol. The Espinosa equation for a molecule in a crystal of **2*** gives the $\text{Sb}\cdots\text{O}(\text{MeOH})$ bond energy equal to -11.3 kcal/mol. This value is higher compared to that in the isolated state as well.

The same DFT and Espinosa methods were used for evaluation of $\text{Sb}\cdots\text{O}(\text{MeOH})$ and $\text{Sb}\cdots\text{O}(\text{H}_2\text{O})$ bonds energy in the $\text{Ph}_3(4\text{-OMe-3,6-Bu}^t\text{-Cat})\text{Sb}\cdot\text{MeOH}$ (**5**) and $\text{Ph}_3\text{CatSb}\cdot\text{H}_2\text{O}$ (**7**) complexes. According to DFT calculations, the bond energy values of the $\text{Sb}\cdots\text{O}(\text{MeOH})$ in **5** and $\text{Sb}\cdots\text{O}(\text{H}_2\text{O})$ in **7** are -7.6 and -7.5 kcal/mol, whereas the correlation equation of Espinosa gives -5.2 and -6.3 kcal/mol, respectively. Thus, energy values from DFT calculations slightly exceed those obtained from the Espinosa correlation equation, and they can be used for the evaluation of the energy of $\text{Sb}\cdots\text{ligand}$ bonds.

It is of interest to compare atomic charges of the SbOCCO fragments in **1***, **1**, **3**, **2**, **2***, and **4** (Table 4). Atomic charges calculated according to AIM theory in **1*** and **1** are correlated to each other. At least, there is no discrepancy in signs. The strongest difference occurs for the Sb(1) atoms: 1.36 e in **1*** and 2.29 e in **1**. The absence of an additionally coordinated molecule of acetonitrile in **3** does not lead to a significant redistribution of charges in the five-membered SbOCCO fragment in comparison with **1*** and **1**.

Thus, our quantum chemical calculations reasonably reproduce the geometrical and topological characteristics of molecule **1*** in crystal. Therefore, results of such calculations can be used for investigation of topological and energetic parameters forming the basis for a prediction of the possibility of reversible binding of dioxygen to unknown Sb(V) catheholate (amidophenolate) complexes.

3. The Charge and/or Orbital Control of Reactions of Reversible Binding of Dioxygen. The analysis of charges of the SbOCCO fragments in **1–4** (Table 4) and **5–11** (Table 5)

Table 4. Net Atomic Charges in the Five-Membered SbOCCO Fragments in **1***, **1**, **3**, **2**, **2***, and **4**

complex		net AIM charge, e				
	Sb(1)	O(1)	O(2)	C(1) [C(19)] ^a	C(2) [C(24)] ^a	
$\text{Ph}_3(4,5\text{-OMe-3,6-Bu}^t\text{-Cat})\text{Sb}\cdot\text{MeCN}$ (1*)	1.36	-0.95	-0.89	0.50	0.49	
$\text{Ph}_3(4,5\text{-OMe-3,6-Bu}^t\text{-Cat})\text{Sb}\cdot\text{MeCN}$ (1)	2.29	-1.17	-1.16	0.49	0.47	
$\text{Ph}_3(4,5\text{-OMe-3,6-Bu}^t\text{-Cat})\text{Sb}$ (3)	2.23	-1.17	-1.16	0.49	0.44	
$\text{Ph}_3(4,5\text{-N}_2\text{C}_4\text{H}_6\text{-3,6-Bu}^t\text{-Cat})\text{Sb}\cdot\text{MeOH}$ (2*)	1.59	-0.80	-0.58	0.30	0.45	
$\text{Ph}_3(4,5\text{-N}_2\text{C}_4\text{H}_6\text{-3,6-Bu}^t\text{-Cat})\text{Sb}\cdot\text{MeOH}$ (2)	2.31	-1.17	-1.17	0.45	0.48	
$\text{Ph}_3(4,5\text{-N}_2\text{C}_4\text{H}_6\text{-3,6-Bu}^t\text{-Cat})\text{Sb}$ (4)	2.25	-1.18	-1.15	0.50	0.44	

^aThe numeration of the SbOCCO fragment for **1*** is in square brackets (see Figure 8b).

Table 5. Net Atomic Charges in the Five-Membered SbOCCO Fragments of **5–11**

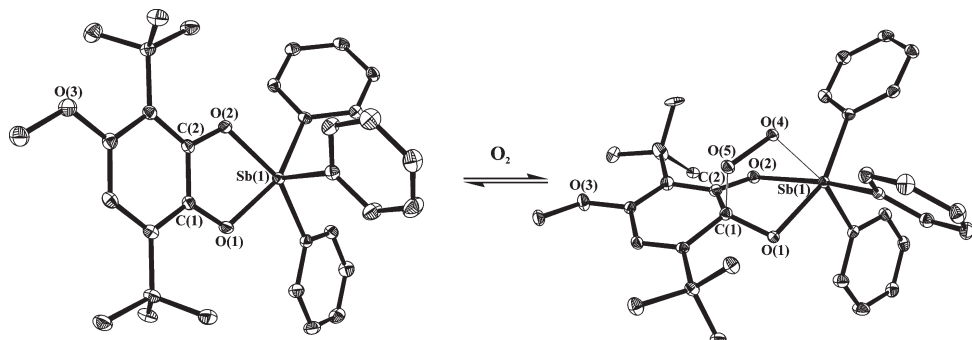
complex	Sb(1)	O(1)	O(2) [N(1)] ^b	C(1)	C(2)
$\text{Ph}_3(4\text{-OMe-3,6-Bu}^t\text{-Cat})\text{Sb}\cdot\text{MeOH}$ (5)	2.29	-1.17	-1.16	0.46	0.45
$\text{Ph}_3(4\text{-OMe-3,6-Bu}^t\text{-Cat})\text{Sb}$ (6)	2.22	-1.16	-1.16	0.45	0.48
$\text{Ph}_3\text{CatSb}\cdot\text{H}_2\text{O}$ (7)	2.23	-1.17	-1.17	0.48	0.45
Ph_3CatSb (8)	2.22	-1.15	-1.18	0.43	0.51
$\text{Ph}_3(3,6\text{-Bu}^t\text{-Cat})\text{Sb}$ (9)	2.23	-1.16	-1.16	0.45	0.46
$\text{Ph}_3(4,6\text{-Bu}^t\text{-AP(2,6-Me-Ph)})\text{Sb}$ (10)	2.18	-1.18	-1.27	0.50	0.29
$\text{Ph}_3(4,6\text{-Bu}^t\text{-AP(2,6-Pri-Ph)})\text{Sb}$ (11)	2.18	-1.18	-1.26	0.50	0.28

^aThe numeration of atoms is shown in Figure 8a. ^bIn **10** and **11**, N(1) atom instead of O(2) atom.

Table 6. HOMO Energies and Atomic Contributions to HOMO in 1–11

complex	E_{HOMO}^a , eV	E_{ox}^b , V	atomic contributions to HOMO ^c , %				
			Sb	O(1)	O(2) [N(1)] ^d	C(1)	C(2)
Ph ₃ (4,5-OMe-3,6-Bu ^t -Cat)Sb·MeCN (1)	−4.871	—	2.12	11.37	10.19	14.43	14.54
Ph ₃ (4,5-N ₂ C ₄ H ₆ -3,6-Bu ^t -Cat)Sb·MeOH (2)	−5.116	—	2.12	12.99	15.02	15.12	14.67
Ph ₃ (4,5-OMe-3,6-Bu ^t -Cat)Sb (3)	−4.980 (−7.293)	0.6	1.94 (1.16)	11.84 (10.74)	7.87 (6.75)	14.50 (16.44)	15.52 (16.70)
Ph ₃ (4,5-N ₂ C ₄ H ₆ -3,6-Bu ^t -Cat)Sb (4)	−5.061 (−7.374)	—	1.61 (1.68)	17.54 (12.89)	9.58 (7.06)	15.66 (17.20)	14.87 (15.17)
Ph ₃ (4-OMe-3,6-Bu ^t -Cat)Sb·MeOH (5)	−4.898	—	1.88	16.03	6.10	17.59	8.46
Ph ₃ (4-OMe-3,6-Bu ^t -Cat)Sb (6)	−4.898 (−7.293)	0.68	2.25 (1.18)	13.64 (10.27)	5.69 (5.85)	18.87 (22.00)	8.25 (9.00)
Ph ₃ CatSb·H ₂ O (7)	−5.306	—	2.42	17.25	15.14	15.41	16.15
Ph ₃ CatSb (8)	−5.225 (−7.565)	—	1.67 (1.34)	11.83 (9.13)	19.59 (15.22)	16.75 (18.18)	16.00 (18.71)
Ph ₃ (3,6-Bu ^t -Cat)Sb (9)	−5.197 (−7.483)	0.76	3.07 (1.26)	12.82 (8.21)	14.63 (15.06)	16.84 (17.76)	16.67 (19.80)
Ph ₃ (4,6-Bu ^t -AP(2,6-Me-Ph))Sb (10)	−4.789 (−7.102)	0.54	1.96 (0.97)	14.86 (10.43)	19.75 (13.81)	16.19 (15.39)	15.07 (14.67)
Ph ₃ (4,6-Bu ^t -AP(2,6-Pr ⁱ -Ph))Sb (11)	−4.789 (−7.102)	0.44	1.63 (1.03)	12.59 (10.96)	16.78 (13.81)	13.34 (15.19)	12.80 (16.29)

^a HOMO energies and atomic contributions to HOMO without parentheses are calculated by DFT, whereas those between parentheses are calculated by HF. ^b Oxidative potentials of the catecholate and amidophenolate complexes. ^c The atomic numeration is shown in Figure 8a. ^d In **10** and **11**, N(1) atom instead of O(2) atom.

Figure 9. The reversible binding of molecular oxygen to Ph₃(4-OMe-3,6-Bu^t-Cat)Sb (**6**).

calculated according to AIM theory has not shown significant differences for complexes with reversible binding (**1–6, 10, 11**) and no binding (**7–9**) of dioxygen. NBO and Mulliken charges do not show the difference for antimony complexes as well. Consequently, there is no obvious charge control for these complexes.

The energies of HOMO (Table 6) in **1–11** were also analyzed in order to find characteristics allowing one to predict a priori the capability to bind reversibly dioxygen to catecholate and amidophenolate complexes of antimony(V). According to calculations, the additional coordinated molecule of acetonitrile in **1** increases the energy of HOMO as compared to the corresponding uncoordinated complex **3**. However, the HOMO energy in **5** as compared to **6** is not changed. The HOMO energy in **2** and **7** is decreased as compared to **4** and **8**. It is noteworthy that HOMO energies E_{HOMO} and the oxidative potentials E_{ox} in **3** and **6** do not correlate to each other. The **3** complex is oxidized more easily than **6**, but the HOMO in **3** lies lower. In order to understand such a discrepancy, the mutual disposition of OMe groups and of the catecholate ligands in **3** and **6** was analyzed.

It should be noted that there are no X-ray data for these complexes; therefore, the geometries of **1** and **5** complexes without additionally coordinated molecules were used to start DFT calculations. According to X-ray data, the dihedral angles between the

catecholate ligand plane and C(21)–O(3)–C(33) [C(22)–O(4)–C(34)] fragment in **1** (Figure 1) are 82.05° (77.04°), whereas the same dihedral angle in **5** is 5.75°. In other words, the OMe group in **5** lies in the catecholate ligand plane, whereas in **1**, it is practically orthogonal. The same tendency is kept after DFT calculations in **6** (1.11°) and **3** (73.16° and 73.82°). Apparently, the disposition of the OMe group in **6** is more preferable for demonstration of π -donor ability as compared to **3**. Therefore, the HOMO energy of **3** lies lower than in **6** according to calculations. However in **6**, the rotation of the OMe group around the C(catecholate)–O(methoxy) bond should be practically free in solution. This can significantly decrease the π -donor ability of the OMe group. The same rotation of two methoxy groups in the 4,5-positions of the catecholate ligand takes place in solution as well. However, such rotation of two methoxy groups should be mutually coordinated for steric reasons. Probably, when one methoxy group is in a favorable position for donation of electron density, the other one is then disposed in unfavorable position. The π -donor ability of one methoxy group decreases upon rotation, whereas the other one increases. Therefore, the oxidative potential in Ph₃(4,5-OMe-3,6-Bu^t-Cat)Sb (**3**) is lower than in Ph₃(4-OMe-3,6-Bu^t-Cat)Sb (**6**).

The energy of HOMO in **3**, **4**, **6**, **10**, and **11** (without additionally coordinated molecules) vary in the range from −4.980 to −4.789 eV, whereas the analogous parameter in **8** and **9**

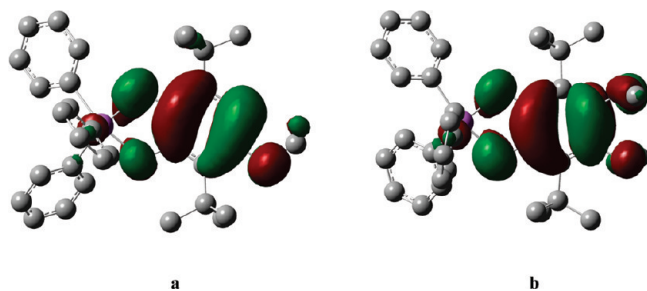


Figure 10. HOMO isosurfaces (0.02 au) in 6 (a) and 3 (b).

are -5.225 and -5.197 eV (Table 6). It should be noted that the HOMO energy in Ph_3SbAP complexes (**10**, **11**) lies higher than that in **3**, **4**, and **6**. The difference of the HOMO energy between complexes with and without reversible binding of dioxygen is 0.136 eV. It should be noted that, according to ^1H NMR monitoring of the **3**, **10**, and **11** complexes, they form corresponding spiroendoperoxides during $1\text{--}2$ h with 100% conversion rate. On the other hand, the conversion rate of **4** and **6** is 37 and 80% , respectively. This allows one to suppose that the HOMO energy of the catecholate complexes of Sb(V) can correlate with the conversion rate of the catecholate complexes in spiroendoperoxide antimony(V) ones. Apparently, the decrease of the HOMO energy as compared to HOMO in **4** will lead to a conversion decrease and stop the process of reversible dioxygen binding. Consequently, the energy value of HOMO between -5.197 and -5.061 eV can serve as a thermodynamic criterion for reversible oxygen binding reactions in catecholate and amidophenolate complexes of Sb(V).

In order to understand if such criterion can be used for other complexes, DFT calculations were carried out for $\text{Ph}_3\text{Sb}(\text{PhenCat})$ (PhenCat, phenanthrene-9,10-diolate), which reversibly binds dioxygen as well. E_{HOMO} in $\text{Ph}_3\text{Sb}(\text{PhenCat})$ is -4.82 eV and the observed conversion rate is 100% .

It is interesting to compare the contribution of atomic orbitals of the C(1) and C(2) atoms to HOMO in **3** and **6** complexes. Complex **3** contains actually two OMe groups in 4,5-positions of the catecholate ligand, whereas complex **6** contains only one OMe group in the 4-position. The contribution of the C(1) atomic orbitals to HOMO is significantly larger than that of the C(2) atom, and the reversible binding of dioxygen to the complex occurs exactly at the C(1) atom (Figure 9). In other words, two different substitutes in positions 4 and 5 (for example, H and OMe in **6**) determine the place of the oxygen attack in substituted 3,6-di-*tert*-butylcatecholate complexes. In disubstituted 3,6-di-*tert*-butylcatecholates complexes (for example, OMe and OMe in **3**), the site of the dioxygen attack is rather statistical. This situation is reflected by the HOMO shapes (Figure 10).

It should be noted that DFT and HF calculations agree with each other in spite of the difference of the HOMO energy values and the contributions of atomic orbitals to HOMO. Thus, we can conclude that this regularity does not depend on the calculation method and has an objective character.

CONCLUSION

We carried out the high-resolution X-ray experiments of $\text{Ph}_3(4,5\text{-OMe-3,6-Bu}^{\text{t}}\text{-Cat})\text{Sb}\cdot\text{MeCN}$ (**1***) and $\text{Ph}_3(4,5\text{-N}_2\text{C}_4\text{H}_6\text{-3,6-Bu}^{\text{t}}\text{-Cat})\text{Sb}\cdot\text{MeOH}$ (**2***) complexes and analyzed them by AIM theory. It was found that the Sb—C(Ph), Sb—O(catecholate), and Sb \cdots N(O) bonds are intermediate, whereas the O—C and C—C

bonds are covalent, respectively. All intramolecular interactions in **1*** and **2*** were analyzed and their energies were evaluated by the Espinosa equation. DFT and HF calculations were carried out for a series of catecholate and amidophenolate complexes. It was shown that these calculations reproduce the geometrical and topological parameters of complexes. Atomic charges and the HOMO energies in antimony(V) complexes were analyzed. A charge control of reactions of reversible binding dioxygen is absent. However, a control of these reactions by atomic orbital energies takes place. It was found that the frontier value of the HOMO energy is within -5.197 to -5.061 eV for dioxygen complexes with or without reversible dioxygen binding. Thus, the HOMO energies can be used as thermodynamic criterion for the prediction possibility of the reversible dioxygen binding to catecholate and amidophenolate complexes of Sb(V). Also, the contribution of the atom orbitals of the carbon atoms in the five-membered metallocycle to HOMO energy in complexes with different substitutes in positions 4 and 5 of the catecholate ligand allows determining exactly the addition place of dioxygen.

EXPERIMENTAL SECTION

The data were collected on a SMART APEX diffractometer (graphite-monochromated, Mo K α radiation, ω - and θ -scan technique, $\lambda = 0.710\,73$ Å) at 100 K. The structures were solved by direct methods and were refined on F^2 using the SHELXTL¹⁷ package. All non-hydrogen atoms were refined anisotropically. SADABS¹⁸ was used to perform area-detector scaling and absorption corrections.

Crystal data for $\text{Ph}_3(4,5\text{-OMe-3,6-Bu}^{\text{t}}\text{-Cat})\text{Sb}\cdot\text{MeCN}$ (**1***): $M = 674.458$, monoclinic, space group $P2_1/n$, $a = 13.5714(3)$ Å, $b = 15.9472(4)$ Å, $c = 15.0811(3)$ Å, $\beta = 97.835(1)$ °, $V = 3233.35(3)$ Å 3 , $Z = 4$, $d_{\text{calc}} = 1.384$ mg·m $^{-3}$, $\mu = 0.891$ mm $^{-1}$, $F(000) = 1392$. Intensities of 157 153 reflections were measured with a Bruker AXS SMART diffractometer (Mo K α , $\varphi-\omega$ -scans, $\theta < 51.0$ °), and 35 018 independent reflections [$R_{\text{int}} = 0.0172$] were used in further refinement. For **1***, the refinement converged to $wR_2 = 0.0684$ and GOF = 1.012 for all observed reflections [$R_1 = 0.0266$ was calculated against F for 29 804 observed reflections with $I > 2\sigma(I)$].

Crystal data for $\text{Ph}_3(4,5\text{-N}_2\text{C}_4\text{H}_6\text{-3,6-Bu}^{\text{t}}\text{-Cat})\text{Sb}\cdot\text{MeOH}$ (**2***): $M = 687.50$, triclinic, space group $\overline{P}\overline{1}$, $a = 10.0526(2)$ Å, $b = 11.8361(3)$ Å, $c = 14.5638(3)$ Å, $\alpha = 88.564(1)$ °, $\beta = 82.172(1)$ °, $\gamma = 68.612(1)$ °, $V = 1597.91(6)$ Å 3 , $Z = 2$, $d_{\text{calc}} = 1.429$ mg·m $^{-3}$, $\mu = 0.902$ mm $^{-1}$, $F(000) = 712$. Intensities of 320 356 reflections were measured with a Bruker AXS SMART diffractometer (Mo K α , $\varphi-\omega$ -scans, $\theta < 51.45$ °) and 35 744 independent reflections [$R_{\text{int}} = 0.0228$] were used in further refinement. For **2*** the refinement converged to $wR_2 = 0.0608$ and GOF = 1.076 for all observed reflections [$R_1 = 0.0227$ was calculated against F for 33 736 observed reflections with $I > 2\sigma(I)$].

The multipole refinement was carried out within the Hansen–Coppens formalism¹⁹ using the MoPro program package.²⁰ Before the refinement, C—H bond distances were normalized to the values obtained in neutron diffraction analyses.²¹ The level of the multipole expansion was hexadecapole for the Sb(1), octupole for all other non-hydrogen atoms, and one dipole for hydrogen atoms. The refinement of compound **1*** was carried out against F and converged to $R = 1.606\%$, $wR = 1.384\%$, GOF = 1.002 for 28 134 merged reflections with $I > 2\sigma(I)$. The refinement of compound **2*** was carried out against F and converged to

$R = 1.589\%$, $wR = 1.576\%$, GOF = 0.999 for 34 482 merged reflections with $I > 2\sigma(I)$. The ratio of the number of reflections to the number of refined parameters was more than 10 for **1*** and **2***. All bonded pairs of atoms satisfy the Hirshfeld rigid-bond criteria.²² Analysis of topology of experimental $\rho(\mathbf{r})$ function was carried out using the WINXPRO program package.²³ The residual electron density was not more than $0.5 \text{ e} \cdot \text{\AA}^{-3}$.

Quantum calculations were carried out using the B3LYP/DZVP and HF/DZVP (method/basis) by Gaussian 03W program.¹⁶ The absence of imaginary frequencies shows that molecules are in minimum of potential energy. Analysis of topology of theoretical $\rho(\mathbf{r})$ function was carried out using the AIMALL program package.²⁴

■ ASSOCIATED CONTENT

Supporting Information. Experimental $\nabla^2\rho(\mathbf{r})$ sections and cif files for **1*** and **2***. This material is available free of charge via the Internet at <http://pubs.acs.org>.

■ AUTHOR INFORMATION

Corresponding Author

*Fax: (+7)8314621497. E-mail: gera@iomc.ras.ru.

■ ACKNOWLEDGMENT

This work was supported by Russian Foundation for Basic Research (Project Nos. 09-03-97034-r_povolzh'e_a) and State Contract No. P-337.

■ REFERENCES

- (1) Abakumov, G. A.; Poddel'sky, A. I.; Grunova, E. V.; Cherkasov, V. K.; Fukin, G. K.; Kurskii, Yu. A.; Abakumova, L. G. *Angew. Chem. Int. Ed.* **2005**, *44*, 2767.
- (2) Cherkasov, V. K.; Abakumov, G. A.; Grunova, E. V.; Poddel'sky, A. I.; Fukin, G. K.; Baranov, E. V.; Kurskii, Yu.A.; Abakumova, L. G. *Chem.—Eur. J.* **2006**, *12*, 3916.
- (3) Abakumov, G. A.; Cherkasov, V. K.; Grunova, E. V.; Poddel'sky, A. I.; Abakumova, L. G.; Fukin, G. K.; Baranov, E. V. *Dokl. Chem.* **2005**, *405* (2), 222.
- (4) Cherkasov, V. K.; Grunova, E. V.; Poddel'sky, A. I.; Fukin, G. K.; Kurskii, Yu. A.; Abakumova, L. G.; Abakumov, G. A. *J. Organomet. Chem.* **2005**, *690*, 1273.
- (5) Pecoraro, V. L.; Baldwin, M. J.; Gelasco, A. *Chem. Rev.* **1994**, *94*, 807.
- (6) Dickman, M. H.; Pope, M. T. *Chem. Rev.* **1994**, *94*, 569.
- (7) Hall, M.; Sowerby, D. B. *J. Am. Chem. Soc.* **1980**, *102*, 628.
- (8) Poddel'sky, A. I.; Smolyaninov, I. V.; Kurskii, Yu. A.; Fukin, G. K.; Berberova, N. T.; Cherkasov, V. K.; Abakumov, G. A. *J. Organomet. Chem.* **2010**, *695*, 1215.
- (9) Bader, R. F. W. *Atoms in Molecules—A Quantum Theory*: Oxford University Press: Oxford, 1990.
- (10) Bushmarinov, I. S.; Lyssenko, K. A.; Antipin, M. Yu. *Russ. Chem. Rev.* **2009**, *78* (4), 283.
- (11) Popelier, P. L. A. *J. Phys. Chem. A* **1998**, *102*, 1873.
- (12) Koch, U.; Popelier, P. L. A. *J. Phys. Chem.* **1995**, *99*, 9747.
- (13) Batsanov, S. S. *Russ. J. Inorg. Chem.* **1991**, *36* (12), 1694.
- (14) (a) Jeffery, G. A. *An Introduction to Hydrogen Bonding*; Oxford University Press: New York, 1997. (b) Desiraju, G. R.; Steiner, T. *The Weak Hydrogen Bond*; Oxford University Press: Oxford, 1999.
- (15) Espinosa, E.; Molins, E.; Lecomte, C. *Chem. Phys. Lett.* **1998**, *285*, 170.
- (16) Frisch, M. J.; Trucks, G. W.; Schlegel, H. B.; Scuseria, G. E.; Robb, M. A.; Cheeseman, J. R.; Montgomery, J. A. Jr; Vreven, T.; Kudin,

K. N.; Burant, J. C.; Millam, J. M.; Iyengar, S. S.; Tomasi, J.; Barone, V.; Mennucci, B. *Gaussian 03, revision C.02*; Gaussian, Inc.: Wallingford, CT, 2004.

- (17) Sheldrick, G. M. *SHELXTL v. 6.12, Structure Determination Software Suite*, Bruker AXS: Madison, WI, 2000.
- (18) Sheldrick, G. M. *SADABS v. 2.01, Bruker/Siemens Area Detector Absorption Correction Program*, Bruker AXS: Madison, WI, 1998.
- (19) Hansen, N. K.; Coppens, P. *Acta Crystallogr.* **1978**, *A34*, 909.
- (20) Jelsch, C.; Guillot, B.; Lagoutte, A.; Lecomte., C. *J. Appl. Crystallogr.* **2005**, *38*, 38.
- (21) Allen, F. H.; Kennard, O.; Watson, D. G.; Brammer, L.; Orpen, A. G.; Taylor, R. *J. Chem. Soc. Perkin Trans. 2* **1987**, S1.
- (22) Hirshfeld, F. L. *Acta Crystallogr., Sect. A* **1976**, *32*, 239.
- (23) Stash, A.; Tsirelson, V. *J. Appl. Crystallogr.* **2002**, *35*, 371.
- (24) Keith T. A. AIMALL, 2008.